Effect of mixing conditions on the wet preparation of ceramic foams

Celani, Andrea; Blackburn, Stuart; Simmons, Mark; Stitt, E. H.

DOI:
10.1016/j.cherd.2018.03.044

Document Version
Publisher's PDF, also known as Version of record

Citation for published version (Harvard):
Celani, A, Blackburn, S, Simmons, MJH & Stitt, EH 2018, 'Effect of mixing conditions on the wet preparation of ceramic foams', Chemical Engineering Research and Design, vol. 134, pp. 1-14.
https://doi.org/10.1016/j.cherd.2018.03.044

Contents lists available at ScienceDirect

Chemical Engineering Research and Design

journal homepage: www.elsevier.com/locate/cherd

Effect of mixing conditions on the wet preparation of ceramic foams

A. Celani[a,b], S. Blackburn[a], M.J.H. Simmons[a,*], E.H. Stitt[b]

[a] School of Chemical Engineering, University of Birmingham, B15 2TT, United Kingdom
[b] Johnson Matthey Technology Centre, Billingham, TS23 1LB, United Kingdom

ARTICLE INFO

Article history:
Received 30 October 2017
Received in revised form 26 March 2018
Accepted 26 March 2018
Available online 4 April 2018

Keywords:
Ceramic foams
Mixing
Aerated stirred vessel
Design of Experiment
Rheology

ABSTRACT

Ceramic foams are a promising alternative to conventional catalyst supports due to their macro-porosity, which should enhance mass transport properties during reactions. Whilst direct foaming is a straightforward production method, the use of kitchen mixers commonly reported in the literature to initially froth the ceramic slurry limits understanding of scale-up. This study reports a systematic experimental investigation of the impact of mixing parameters on the properties of the foams produced in an agitated baffled vessel of diameter, T = 175 mm, equipped with an up-pumping pitch blade turbine with diameter of either D = 0.23 T or 0.51 T and a bottom round sparger with a diameter of 45 mm. The flow conditions in the present study were in the low to mid transitional regime ($50 < Re < 1000$). Design of Experiments (DoE) was employed to generate a series of screening experiments by variation of sparging time, air flow rate, impeller speed and impeller diameter. The mixing behaviour was described as a function of relevant dimensionless groups (Re, Fr, Fl_g, etc.) whilst the gas–liquid flow regime was estimated by examination of a ceramic particles free system. The properties of the foams obtained were correlated with key dimensionless numbers, though the exponents obtained deviated from values in the published literature. In addition, the rheology of the foam was correlated to the bubble size distribution showing that rheology measurements have potential for at-line measurement to control the structure of the produced material.

1. Introduction

The direct foaming of a ceramic slurry is a simple and versatile method to generate macroporous ceramic materials. These can be used as refractory insulators, filters for molten metals filtration and catalyst supports (Gauckler et al., 1985; Colombo and Sheffled, 2005). The structural properties of these materials are influenced by the formulation of the initial ceramic slurry: in particular, the amphiphile structure and concentration, the solid percentage and the operational pH play a significant role. Gonzenbach et al. (2007) reported an increase in foam porosity as the amphiphile concentration was increased due to the higher particle hydrophobicity as the amount of amphiphile adsorbed at the particle surface increases. Amphiphile concentration also has an effect on bubble size with a reduction in bubble dimensions as the concentration of the amphiphile is increased (Gonzenbach et al., 2006). The percentage of solid in the initial slurry influences both the foam porosity and bubble size. Gonzenbach et al. (2007) observed a reduction in bubble size and porosity as the solid percentage was increased; they suggested that the decrease in porosity was due to the higher viscosity of the suspension that in turn hindered the air entrainment within the suspension. Finally, pH affects both the particle stabilization in the initial slurry and the dissociation of the functional group of the amphiphile, with the ideal pH reported to be equal to the pKa of the functional group (Gonzenbach et al., 2007; Studart et al., 2006).

Although the formulation of the initial ceramic slurry and its relationship with the structural properties of the foam has been widely

* Corresponding author.
E-mail address: m.j.simmons@bham.ac.uk (M.J.H. Simmons).
https://doi.org/10.1016/j.cherd.2018.03.044

investigated, little attention has been given to the manufacturing process. In the literature, the usage of a kitchen mixer is normally reported to mechanically froth the ceramic slurry (Gonzenbach et al., 2007; Gonzenbach et al., 2006; Wong et al., 2011) which presents limitations in term of process scale-up since key mixing parameters such as power input and flow field cannot be easily correlated or extrapolated to industrial scale equipment.

The objective of this study is to gain an understanding of how mixing parameters impact the structure of a ceramic foam slurry produced in a sparged vessel which is more representative of an industrially used process. In order to determine which parameters were statistically significant in affecting the properties of the forms formed, a Design of Experiments (DoE) approach was employed. The investigated parameters were impeller diameter (D), impeller speed (N), gas flow rate (G), sparging time (t) and mean pore size of the sparging disks ($\bar{d}$). These factors were changed between two different values to develop a wide range of foam properties. The significant parameters, once identified, were related to the foam properties (e.g. porosity, bubble size distribution) using global mixing parameters. The correlation of system properties to dimensionless groups is well-established in chemical engineering, for example the relationship between the Sauter mean diameter of drops and the Weber number in emulsions (Shinnar, 1961; Calabrese et al., 2000) and the correlation between gas hold-up and superficial gas velocity in slurry bubble columns (Bach and Pilhofer, 1978; Hikita et al., 1980; Hughmark, 1967). These correlations were applied to wet foams to give deeper insight into the effects of mixing and process variables on the preparation of the foam precursors. Foam rheology was correlated to the structure of the foams produced under different mixing conditions, suggesting the possibility of using this technique as an at-line measurement to control the structure of the produced foams.

2. Materials and methods

2.1. Materials

Fumed Al_2O_3 particles (AEROXIDE AluC) were obtained from Evonik Industries (Essen, Germany). The alumina was crystalline with a γ/δ- structure. Density and surface area were 50 g L^{-1} and 85–115 m^2 g^{-1} respectively. Butyric acid obtained from Alfa Aesar (Heysham, United Kingdom) was used to modify the particle surface properties. Potassium hydroxide solution 40%$_{v/v}$, prepared by dissolving potassium hydroxide pellets (Alfa Aesar, Heysham, United Kingdom) in demineralized water, and nitric acid 70%$_{v/v}$ (Alfa Aesar, Heysham, United Kingdom) were used to adjust the suspension pH.

2.2. Suspension preparation

Alumina suspensions were prepared by stepwise addition of the powder to an acidic solution while being continuously stirred using an overhead mixer. The pH of all suspensions was adjusted to electrostatically stabilise the particles. The isoelectric point of alumina occurs between pH 7–10 depending on the type of alumina (Kasprzyk-Hordern, 2004). The suspension solid loading and pH were set to 20%$_{w/w}$ (83%$_{v/v}$) and 4.70 respectively. In a typical formulation, 1.1 kg of alumina was added to 4.425 L of demineralized water containing 75 mL of 70%$_{v/v}$ HNO_3. 155 mL of butyric acid was added to the suspension to modify the surface properties of the ceramic precursor. After amphiphile addition, the suspension pH was adjusted to 3.50 through the addition of 40%$_{v/v}$ KOH.

2.3. Suspension foaming

Foaming of 4.5 L suspension was carried out in a 5 L stainless-steel vessel having a diameter, T = 175 mm. The vessel was fitted with four vertical baffles of width T/10 and with a circular gas sparger having a diameter of 45 mm fitted 20 mm from the bottom of the vessel whilst the disk-impeller clearance was 30 mm. Two different metal sintered sparging disks (ASCO Filtri s.r.l., Binasco, Italy) were used with an average pore size of 40 μm and 100 μm respectively. During foaming, depending on the experiment being carried out, the slurry was agitated with an up-pumping pitch blade turbine having a diameter, D, of either 40 mm or 90 mm. A gas flow rate equal to 2 L min^{-1} and 20 L min^{-1} and a sparging time of 1 min and 20 min were used. The impeller Reynolds number varied between 50 and 1000 depending upon the operating conditions; the values were calculated using the viscosity of the initial alumina suspension. The shaft torque was recorded by attaching a Binsfeld Engineering Inc. Torque Trak 10 K strain gauge to the impeller shaft. The density of the foam was determined by weighing a known volume of foam. Some of the wet foam was stored in a sealed graduated container to assess its stability; the foam was left for two weeks and the change in volume was noted. The rest of the foam was dried at 80 °C for 2 h in a Carbolite Furnace CWF. The dry foam was calcined at 600 °C for 4 h. During the ramping step and for the first 45 min the furnace was purged under N_2 while after the furnace was run under air. The heating rate was 2 °C min^{-1}.

2.4. Determination of foam porosity

To determine the porosity of the calcined foam, a water pick-up experiment was carried out. The initial weight of four foam lumps was recorded then these were submerged in water and the weight of the wet lumps was recorded for four days. The average amount of water picked up was determined by difference between the weight of the wet foam and its initial weight. From this value the foam porosity and pore volume were calculated.

2.5. Foam bubble size measurement

The mean bubble size was expressed in terms of Sauter mean diameter (Merkus, 2009). Direct imaging of the bubbles in the wet three phase foam was not possible; consequently, the bubble size was determined by image analysis of cross sections cut from the dried and calcined foams. The drying, sectioning and processing led to uncertainties in the accuracy of the bubble size present in the foam during mixing. However, all measurements were made in the same way and thus the error would be systematic in nature allowing comparison between foams. Foam bubble size distribution was determined by acquiring optical microscope images (Nikon Eclipse E200) of cross sections of the foams under investigation. Bubble diameters were obtained by analysing the acquired images with Fiji ImageJ 1.50a (Wayne Rasband, National Institute of Health, USA). Fig. 1(a) shows an example of the cross-sectional image of one of the produced foam while Fig. 1(b) shows a binary image of the same image as Fig. 1(a). The binary images were used to determine the bubble size; it should be noted that only the bubbles that were in focus were analysed. The distributions were corrected by dividing the cross sectional diameter by 0.79 to account for the random position of the bubbles during sample sectioning. The correction factor was determined by Williams et al. (2008). Typically, due to the rate of data acquisition, 100 bubbles were measured per sample. Although this ultimately limited the accuracy and precision of the data it did allow comparisons to be made; the bubble size confi-

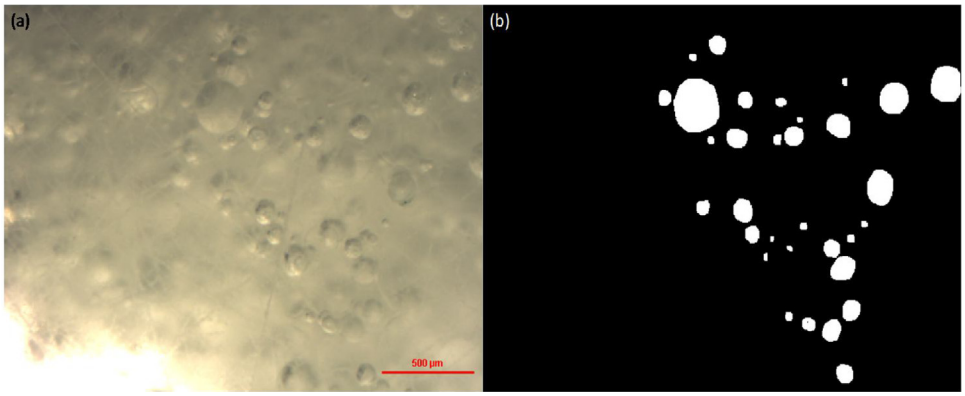

Fig. 1 – Example of cross-sectional image for one of the produced foam: (a) optical microscope image, (b) thresholded image.

dence interval was determined using the procedure of Buffo and Alopaeus (2016).

2.6. Foam rheology measurement

Foam rheology was measured using an AR2000 rheometer (TA Instruments, Brusselsesteenweg, Belgium). The rheological measurements were carried out using a 40 mm acrylic hatched parallel plate (geometry inertia = 1.56 μN m s^2) with the geometry gap set to 500 μm. To check for the occurrence of slip, two further geometries were employed: a 40 mm steel parallel plate (geometry inertia = 8.30 μN m s^2) and a standard size vane-rotor with stator inner radius 15 mm and rotor outer radius 14 mm (geometry inertia = 2.44 μN m s^2). The gap was set to 500 μm and 4000 μm when the parallel plate and the standard vane geometry were employed respectively. Flow curves and viscoelasticity were measured with all the experiments conducted at 20 °C. The sample was firstly equilibrated for 2 min and then pre-sheared at 900 s^{-1} for 30 s. In the upward ramp, the shear rate was increased from 10^{-3} s^{-1} to 1000 s^{-1}, a log ramp mode was used with 10 points per decade acquired every 20 s. The same procedure was followed in the downward ramp were the shear rate was varied from 1000 s^{-1} to 10^{-3} s^{-1}. The selected shear rate range includes the shear rate at which the foam is usually subjected during the foaming experiment; this ranges between 30 and 180 s^{-1} depending upon the operating conditions. To assess the viscoelasticity of the sample an oscillation experiment was carried out. The typical procedure included equilibration of the sample for 2 min followed by a stress sweep step where the oscillation stress was varied from 0.1 Pa to 1000 Pa. The oscillation frequency was equal to 1 Hz and a log ramp mode was used to increase the stress value with 10 points per decade being acquired.

2.7. Design of Experiments (DoE)

A half factorial design with five factors and two levels was employed to screen the significance of the different parameters. Parameter levels were selected through scoping experiments where the parameters were set to their lower and higher values to ensure that an appropriate range of foam properties could be obtained. The screening design generated 16 runs to investigate the effect of independent factors, including impeller diameter D (40–90 mm), impeller speed N (200–1000 rpm), gas flow rate G (2–20 L min^{-1}), sparging time t (1–20 min) and sparging disk mean pore size $\bar{d}$. (40 and 100 μm). Foam porosity, foam density, foam stability and foam bubble size distribution were selected as responses; Table 1 shows the 16 runs with the factors levels and the measured responses. Foam stability is not included in the table since it was observed that it was not affected by the manufacturing process.

3. Theory

It is important to remark that the flow conditions in the present study are low to mid transitional (50 < Re < 1000). Since correlations in this regime cannot be found in the literature, in this work only the correlations from other regimes that gave the best fit are presented. Correlations developed in the turbulent regime were found to give the best fit for the gas hold-up and bubble size correlations whilst, in the absence of a superior approach, the Metzner–Otto correlation was used to determine the impeller mean shear rate.

3.1. Gas hold-up correlations

In the literature, it has been reported that the gas hold-up is affected by gas/liquid/solid physical properties (Ozturk et al., 1987; Bhaga et al., 1971; Sada et al., 1983), operating variables (e.g. pressure, temperature, superficial gas velocity) (Zou et al., 1988; Benhkish et al., 2007; Lau et al., 2004), reactor size (Kastanek et al., 1984; Sarrafi et al., 1999) and type of gas distributor (Wilkinson et al., 1992; Heijnen and Van't Riet, 1984) and several correlations based on these parameters have been proposed. Greaves and Barigou (1990), who studied gas hold-up in large vessels (1–2.7 m) equipped with six blade disc turbines proposed the following:

$$\varepsilon_g = 4.07(N)^{0.62}(Q_g)^{0.64}(D/T)^{1.39} \quad (1)$$

where N is the impeller speed, Q_g is the gas flow rate, D is the impeller diameter and T is the tank diameter. They observed that there is a wide divergence in prediction for different system configurations and operating conditions; they attributed this lack of agreement to the exclusion of the dependence of the gas hold-up on the different flow regimes that could occur under different operating or geometric conditions. These flow regimes were originally proposed by Nienow et al. (1978): at low N the gas passes through the agitator without dispersion and the liquid flows around the outer part of the blades; in this case the impeller is said to be flooded. As the impeller speed is increased beyond the flooding speed N_f the gas is captured by the vortex behind the blades and the impeller is said to be loaded; in this situation, the gas is dispersed and P_g (power consumption of the gassed system) decreases due to the formation of larger cavities. A further increase in N causes the

Table 1 – Half factorial design runs with factors levels and response values.

Run #	Air flow rate (L min^{-1})	Impeller speed (RPM)	Sparging time (min)	Impeller diameter (cm)	Sintered disk mean pore size (μm)	Density (g mL^{-1})	Porosity %	d_{32} (μm)
1	2	200	1	4	100	1.17	82.18	367
2	2	200	20	9	100	0.55	88.68	150
3	20	1000	1	9	40	0.8	88.65	96
4	20	1000	20	4	40	0.36	95.71	189
5	2	1000	1	4	40	0.91	83.42	236
6	2	1000	20	9	40	0.56	95.13	59
7	20	200	1	9	100	1.02	84.63	169
8	20	200	20	4	100	0.56	89.75	240
9	2	1000	20	4	100	0.86	89.71	91
10	20	200	1	4	40	1.02	83.24	331
11	20	200	20	9	40	0.58	91.32	175
12	2	1000	1	9	100	0.92	86.64	129
13	20	1000	20	9	100	0.3	96.71	86
14	20	1000	1	4	100	0.73	86.39	114
15	2	200	1	9	40	1.09	83.43	93
16	2	200	20	4	40	0.96	85.84	384

cavities to change into "vortex" cavities. N_{CD} is the impeller speed at which the gas becomes completely dispersed in the whole vessel while at N_R gross recirculation of gas into the agitator commences.

Smith (1991) used a similar approach to Greaves and Barigou (1990) to predict the gas hold-up correlation; but in this case the extent of gas dispersion was attributed to the different flow regimes. The correlation suggested by Smith (1991) is illustrated below:

$$\varepsilon_g = 0.85(ReFrFl_g)^{0.35}(D/T)^{1.39} \quad (2)$$

where Re is the impeller Reynolds number ($Re = \frac{ND^2\rho}{\mu}$), Fr is the Froude number ($Fr = \frac{N^2D}{g}$) and Fl_g is the gas flow number ($Fl_g = \frac{Q_g}{ND^3}$). Smith (1991) proposed that, except for small tanks (T < 0.44 m), gas hold-up can be predicted using dimensionless numbers. Rewatkar et al. (1993) investigated the effects of different sparger types and positions on the gas hold-up proposing the following correlation:

$$\varepsilon_g = 3.54(D/T)^{2.08}(Fr)^{0.51}(Fl_g)^{0.43} \quad (3)$$

Despite the number of available correlations, one of the most frequently used is that based upon the power dissipated in the system:

$$\varepsilon_g \propto (P_g/V)^A v_s{}^B \quad (4)$$

where P_g is the power consumption of the gassed system, V is the liquid volume and v_s is the superficial gas velocity. Values of A and B range from 0.2 to 0.7 with the tendency for A to be higher for non-coalescing systems (e.g. solutions of electrolytes) compared to coalescing (e.g. pure liquids). Whitton and Nienow (1993) proposed A and B values of 0.26 and 0.66 respectively while Yawalkar et al. (2002) proposed values of 0.25 and 0.41 respectively. It is important to consider that the gas hold-up can be very different in real systems with compared to pure liquids. In addition, bubble diameter may change due to adsorption, desorption and evaporation meaning that these correlations are not universally applicable. However, since ε_g is controlled by bubble size and the amount of recirculating gas, which are functions of both (P_g/V) and v_s, the basic form of (4) appears reasonable (Harnby et al., 2001).

3.2. *Bubble size correlations*

Different models to correlate the drop size to the process variables have been suggested in the literature; these correlations were commonly derived for emulsions but they can be applied to gas–liquid systems. Kolmogoroff proposed that the eddies in the turbulent flow give rise to different stresses depending on their size relative to the Kolmogoroff scale, λ_k, which is expressed by:

$$\lambda_k = \left(\frac{\nu^3}{\varepsilon}\right)^{1/4} \quad (5)$$

where ν is the kinematic viscosity of the continuous phase and ε is the average dissipation usually expressed as $\varepsilon = \frac{P}{V\rho}$ (Pinelli et al., 2001; Montante and Magelli, 2005; Khopkar et al., 2006). The turbulent eddies will give rise to different stresses depending on their size relative to the Kolmogoroff scale. Drop breakage will occur if the pressure across the drop exceeds the pressure due to surface tension holding the drop together (Kolmogoroff, 1949) (turbulent inertial break-up) and, for eddy sizes, where $\lambda \gg \lambda_k$, the following relationship is valid:

$$(d_d)_{max} = c\left(\frac{\sigma}{\rho_c}\right)^{0.6}\varepsilon^{-0.4} \quad (6)$$

where c is a constant, σ is the interfacial tension, ρ_c is the density of the continuous phase and ε is the mean energy dissipation rate. Eq. (6) can also be expressed in the form of dimensionless groups:

$$d_{32}/D = AWe^{-0.6} \quad (7)$$

where A in this case A is equal to $CP_0{}^{-0.4}$. The Weber number (We) is used for analysing the fluid flow when there is an interface between two different fluids with strongly curved surfaces and it is a measure of the relative importance of the fluid inertia compared to its surface tension (Frohn and Roth, 2000); the Weber number in agitated vessels is expressed as:

$$We = \frac{\rho_c N^2 D^3}{\sigma} \quad (8)$$

This theory was originally employed by Hinze (1955) for dilute liquid/liquid systems and was later adopted for

gas/liquid systems (Machon et al., 1997a). It is important to note that, for bubbles smaller than λ_k, viscosity also affects the fluctuating eddy velocity and the following relationship for the turbulent viscous break-up has been proposed by Sprow (1967):

$$\frac{d_{max}(\mu_c \varepsilon \rho_c)^{1/2}}{\sigma f(\frac{\mu_d}{\mu_c})} = const. \quad (9)$$

Eqs. (6) and (7) satisfactorily correlate the effect of surface tension and agitation conditions on bubble/drop size in the case of liquid–liquid systems while discrepancies are observed in the case of gas–liquid systems (Machon et al., 1997b). Acceptable correlations were obtained in gas–liquid systems where bubble coalescence was reduced (e.g. protein solutions) but, in every case, very different values of both the correlating coefficient and the exponent were required to predict the correct value of the mean bubble size (Hu et al., 2003; Hu et al., 2005). Machon et al. (1997a) and Nienow et al. (2003) suggest that the proposed relationships differ because the Weber number only relates to bubble breakage while, in gas–liquid systems, bubble size is determined by a balance between breakage and coalescence. It is evident that, reducing the contribution of coalescence in the gas–liquid systems, leads to better predictions of the bubble size when relationships (6) and (7) are used.

3.3. *Rheology models*

The rheology of the produced foams will be investigated and correlated to its structural properties. In this section the rheology models used to describe the foam rheological behaviour are introduced. Fluids can be classified as either Newtonian or non-Newtonian, depending on whether they obey Newton's law of viscosity, expressed as:

$$\tau = \mu\dot{\gamma} \quad (10)$$

where τ is the shear stress, μ is the viscosity and $\dot{\gamma}$ is the shear rate. Non-Newtonian fluids may be classified as either time independent, including shear-thinning (pseudoplastic) and shear-thickening (dilatant) fluids or time dependent, which include thixotropic and rheopectic liquids as well as viscoelastic materials (Paul et al., 2004).

Ceramic foams may be considered as viscoelastic fluids with both a time dependent and shear dependent thinning behaviour and only a description of the relationships describing this class of fluids will be given. Shear thinning fluids present a decrease in viscosity when the shear rate is increased from low to high levels; their behaviour can be described by different constitutive laws but power law is commonly used:

$$\tau = k\dot{\gamma}^n \quad (11)$$

where k is the fluid consistency index and n is the flow behaviour index; this assumes values less than 1 for shear thinning fluids. However, for ceramic foams, a yield stress exists; below this value the interfacial and inter-particle forces prevent fluid motion ("infinite" viscosity). For shear stresses above the yield stress, the external forces are strong enough to overcome these and the foam flows. These materials can be described by the Herschel–Bulkley constitutive law:

$$\tau = \tau_y + k\dot{\gamma}^n \quad (12)$$

where τ_y is the yield stress. Ceramic foams present a viscoelastic behaviour so a brief description on how to measure this property will be given. Purely elastic materials, can be described by a Hookean spring and their response to an oscillating strain can be expressed by the following stress function:

$$\tau = G\gamma_0 sin(\omega t) \quad (13)$$

where G is the elastic modulus, γ_0 is the maximum strain exerted on the spring, ω is the angular velocity and t is the time. In the case of elastic fluids, strain and stress are in-phase with each other with the strain and stress presenting their maximum at the same time. Purely viscous materials, can be described by a dashpot and their response to an oscillating strain can be described by:

$$\tau = \eta\omega\gamma_0 \cos(\omega t) \quad (14)$$

Visco-elastic fluids can be described by the Kelvin–Voigt model which combines a dashpot and a spring in parallel; the equation of state to describe this model is:

$$\tau = G\gamma_0 \sin(\omega t) + \eta\omega\gamma_0 \cos(\omega t) \quad (15)$$

Real visco-elastic fluids are obviously more complex than the Kelvin–Voigt model and it is common to use the term complex modulus G* to describe them which represents the total resistance of the substance against the applied strain; this is defined as:

$$G^* = G' + iG'' = \tau_0(t)/\gamma_E(t) \quad (16)$$

where G′ and G″ are the storage modulus and the loss modulus respectively. The storage modulus indicates that the stress energy is temporarily stored during the test but that it can be recovered afterwards while the loss modulus indicates that the energy which has been used to initiate the flow is irreversibly lost.

4. Results

4.1. *Determination of process parameters affecting foam structure*

The DoE responses summarized in Table 1 were analysed using JMP 10 software (SAS Institute Inc.) to determine the process factors that affect the foam properties.

Table 2 lists the parameters affecting the different foam properties. Five columns are presented. In the first column, the factors and the factor interactions are listed, the second column shows the contrast value that, in the case of an orthogonal design, is the same as the regression parameter estimates. The third column lists the Lenth t-ratio which is used for the calculation of the individual and simultaneous p-values; this is obtained by the ratio between the contrast value (second column) and the Lenth's Pseudo-Standard Error (PSE). The latter is calculated by Lenth's method which identifies inactive effects from which it constructs an estimate of the residuals standard errors (PSE) (Lenth, 1989). The last

Table 2 – Process parameters affecting foam properties.

Parameter	Contrast	Lenth t-ratio	Individual p-value	Simultaneous p-value
Density				
Sparging time	−0.183	−3.91	0.0074	0.0682
Air flow rate	−0.103	−2.20	0.0489	0.3726
Impeller speed	−0.094	−2.01	0.0624	0.4768
Porosity				
Sparging time	3.159	4.07	0.0063	0.0581
Impeller speed	1.848	2.38	0.0367	0.2910
Air flow rate	1.568	2.02	0.0617	0.4712
Impeller diameter	1.416	1.83	0.0830	0.5917
Bubble size				
Impeller speed	−209.491	−9.49	0.0004	0.0080
Impeller diameter	−87.032	−3.94	0.0072	0.0660
Sparging time & air flow rate	−82.409	−3.73	0.0088	0.0792
Impeller diameter & sintered disk	178.843	8.10	0.0004	0.0041

two columns list the individual and simultaneous p-values respectively. The individual p-value is an indication of the significance of the considered factor; if the factor's individual p-value has a value lower than 0.05 it can be considered a significant factor. The p-values are generated via a Monte Carlo simulation of 10,000 runs of n-1 purely random values and Lenth's t-ratios are produced for each set. The p-value is the interpolated fractional position among these values in descending order. The simultaneous p-value is the interpolation along the max(|t|) of the n-1 values across the runs (Anon, 2012; Ye and Hamada, 2000).

Sparging time, impeller speed and air flow rate were the factors affecting foam density and foam porosity while foam bubble size was governed by impeller speed, impeller diameter and a series of factor interactions between sparging time and air flow rate and between impeller diameter and sintered disk porosity. This study shows the significance of all the considered factors in developing the structure of ceramic foams. Based on this study, the foam properties were correlated to different global mixing parameters.

4.2. *Gas hold-up correlations applied to ceramic foams*

A parallelism can be drawn between the porosity of the wet foam and the gas hold-up in bubble columns. A similar approach has been applied in the case of wet foams, where their porosities were correlated to a series of mixing parameters such as energy dissipation (P_g/V), Reynolds number (Re), Froude number (Fr) and gas flow number (Fl_g); in particular, Eq. (2) was used to correlate foam porosity to the dimensionless group. It is important to note that this correlation was obtained for pure gas–liquid systems under steady state conditions while, in the current study, a three-phase unsteady system (e.g. solid–gas–liquid) was present and divergences from the aforementioned relationship are to be expected. Fig. 2 shows the foam porosity as a function of the dimensionless group ($ReFrFl_g$) for foams produced using different entrainment times. Due to the transient nature of the system and the consequent change in the slurry physical properties (e.g. density and viscosity), dimensionless numbers such as the Reynolds number were calculated using the initial physical properties of the ceramic slurry. The Reynolds number, in particular, is expected to decrease in value during the foaming due to a decrease in density and increase in viscosity. In addition, the impeller speed was varied subjecting the slurry to different shear rates; this resulted in different alumina slurry viscosities due to its non-Newtonian nature.

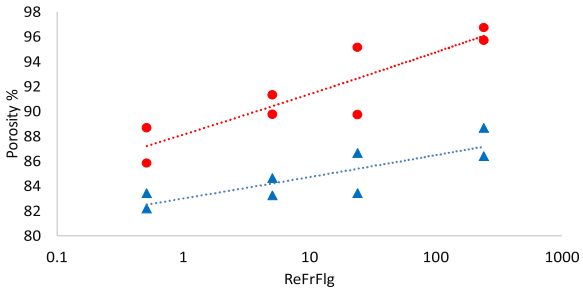

Fig. 2 – Foam porosity as a function of the dimensionless group ($ReFrFl_g$) for foams produced using different sparging times and impeller diameters. T = 1′ (●) and T = 20′ (▲).

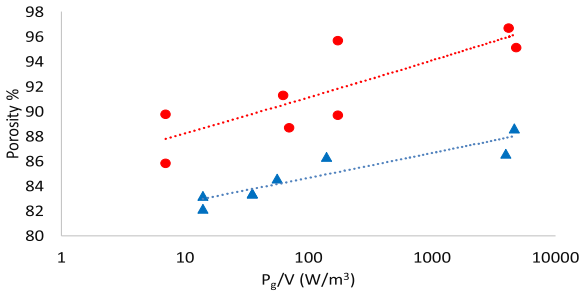

Fig. 3 – Foam porosity as a function of mean energy dissipation for foams produces using different air entrainment times. T = 1′ (●) and T = 20′ (▲).

The average impeller shear rate was determined using the Metzner–Otto correlation ($\dot{\gamma}_A = k_s N$); with the impeller used characterized by a mixer shear constant k_s of 12 (Albright, 2009). Since the viscosity of the ceramic slurry is shear rate dependent, these average shear rates were used to interpolate the viscosity curve of the starting alumina suspension and determine its viscosity at the different operating conditions.

As a result of foam porosity being strongly affected by sparging time, different correlations were derived for foams produced using different entrainment times. Fig. 2 shows a monotonic correlation in all cases (R^2 equal to 0.80 and 0.69 for foam produced a 1′ and 20′ air entrainment time respectively) but, as expected, the exponent of the dimensionless group significantly differed from that proposed by Smith (1991). It has been previously shown that the gas hold-up is more usefully expressed as a function of the mean power dissipation; Fig. 3 shows foam porosity as a function of the mean power dissipation for foams produced using different air entrainment times.

Table 3 – Comparison between exponent values for correlations to determine porosity (gas hold-up) reported in the literature with the values found in this study.

Correlation	Parameter & exponent	Literature value	Value from this study
Smith (1991) Eq. (2)	$ReFrFl_g^{\alpha}$	$\alpha = 0.35$	$\alpha = 0.012 \pm 0.005$
Whitton and Nienow (1993) Eq. (4)	$(P_g/V)^A$	$A = 0.26$	$A = 0.012 \pm 0.003$
Yawalkar et al. (2002) Eq. (5)	$(P_g/V)^A$	$A = 0.25$	

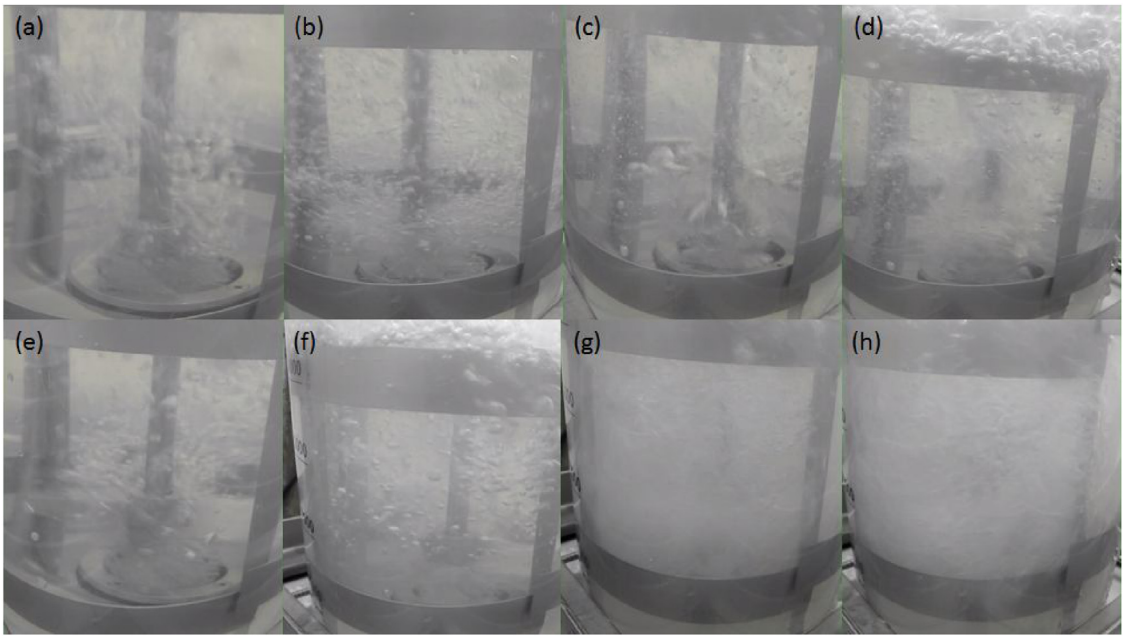

Fig. 4 – Flow regimes at different impeller speed, impeller diameter and gas flow rate. (a) D = 4 cm, G = 2 L/min, N = 200 rpm (b) D = 4 cm, G = 2 L/min, N = 1000 rpm (c) D = 4 cm, G = 20 L/min, N = 200 rpm (d) D = 4 cm, G = 20 L/min, N = 1000 rpm (e) D = 9 cm, G = 2 L/min, N = 200 rpm (f) D = 9 cm, G = 2 L/min, N = 1000 rpm (g) D = 9 cm, G = 20 L/min, N = 200 rpm (h) D = 9 cm, G = 20 L/min, N = 1000 rpm.

Monotonic relationships were found for the evaluated foams (R^2 equal to 0.68 and 0.85 for foam produced a 1′ and 20′ air entrainment time respectively) but again the exponent values were significantly different from the correlations determined for gas–liquid systems. In both the applied correlations, the exponent values were close to 0.3 while in this study the exponent values were in the range 0.012 ± 0.003. Table 3 summarises the values of the exponents reported in the literature and the values proposed in this work.

The foam porosity was correlated to the different flow regimes present under the different operating conditions applied. Since a flow-regime map for an up-pumping pitched blade turbine was not found in the literature, this was determined experimentally keeping in mind that the flow patterns proposed by Nienow et al. (1978) are for gas–liquid systems. The presence of particles in the work undertaken here prevented the visual observation of the flow patterns. In addition, the rheological properties change during the foam formation process and this process could lead to transient flow patterns. Despite not being able to establish visually the flow regime in our system, an indication was obtained by using the experimental process parameters (e.g. impeller speed, impeller diameter and gas flow rate) in a particle free air–liquid (water plus additives) system. From Fig. 4 it was observed that, with the exception of case (b) where a loading pattern is observed, flooding was present when the smaller impeller was used (a,c,d); whereas in larger impeller, when increasing the gas flow rate, a transition from a loaded to a recirculating regime was observed (e–h).

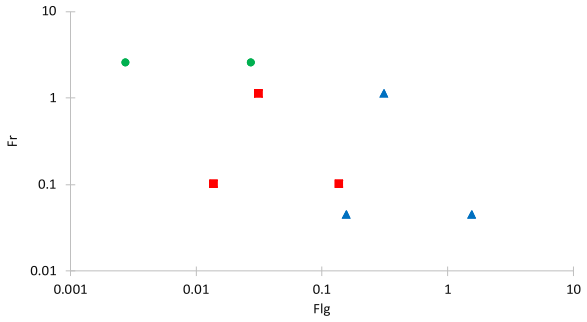

Fig. 5 – Flow regime map for the experimental system representing the different flow regimes: flooded (▲), loaded (■) and fully recirculated (●).

From the visual observation of the different flow regimes, a flow regime map was drawn for the current system by plotting the gas flow number Fl_g (abscissa) and the Froude number Fr (ordinate) in Fig. 5. The aim of this work was not to define an exact flow regime map for the impeller used; the observed flow regimes were plotted as a function of Fr and Fl_g number in order to have an indication of the operating conditions at which they occurred. The limited number of experiments do not allow absolute definition of transition regions between regimes.

Fig. 6(a) and (b) show the foam porosity as a function of the different flow regimes; the different colours and shapes of the bars indicate the flow regimes at which the specific foams were produced. Two different graphs were plotted for the short

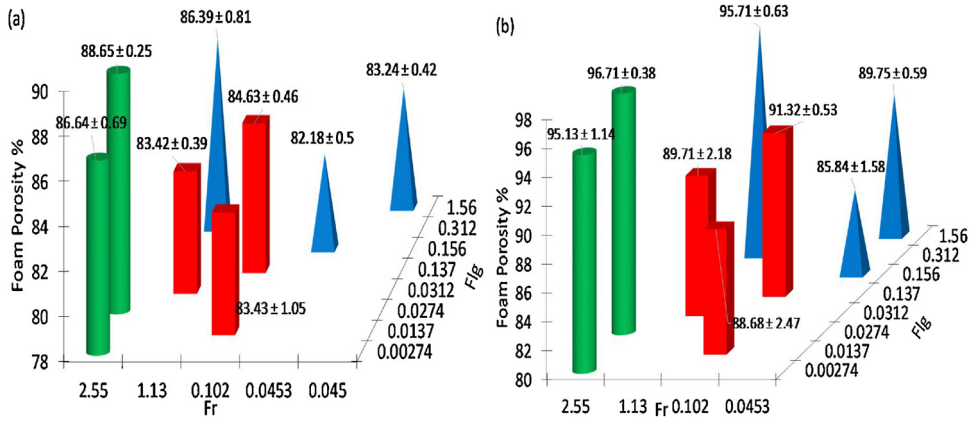

Fig. 6 – Foam porosity as a function of the flow regime conditions for (a) 1 min air entrainment time (b) 20 min air entrainment time. The different flow regimes are represented as flooded (▲), loaded (■) and fully recirculated (●).

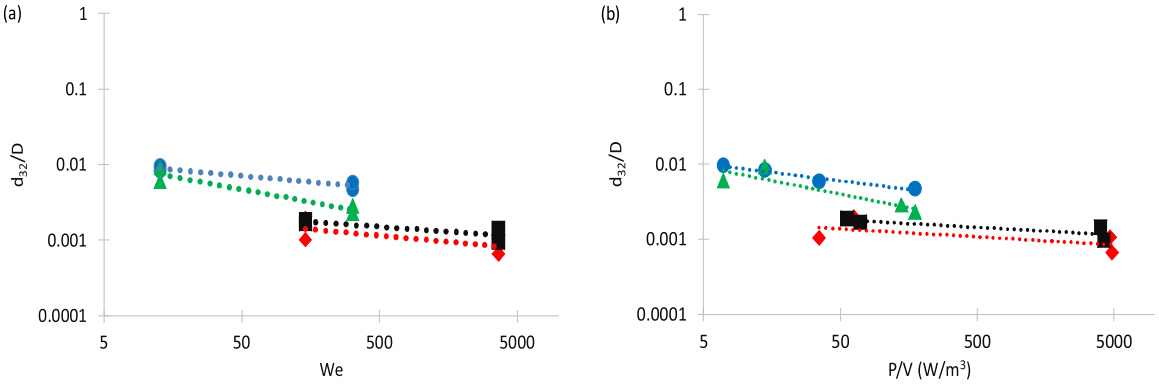

Fig. 7 – d_{32}/D as a function of mean energy dissipation for (a) *We* (b) P_g/V. The different sparger pore size and impeller diameter are indicated as: 40, D = 4 cm (●); 40, D = 9 cm (♦); 100, D = 4 cm (▲); 100, D = 9 cm (■).

and long air entrainment time since that variable affected the foam porosity.

From Fig. 6 it can be noted that a similar trend is followed for both the short and long air entrainment time, with the highest porosity observed when the foam is produced under fully recirculating conditions. It can be noted that, at both air entrainment times, a point characterized by high porosity is present in the flooded region. This point occurs at high Fr and Fl_g numbers which correspond to operating conditions where high flow rate and high impeller speed are used resulting in higher air entrainment and hence porosity. As discussed in Section 4.1, air entrainment time has an effect on the foam porosity; it can be noted that all the foam produced at longer entrainment times had consistently higher porosity values.

4.3. *Bubble size correlations applied to ceramic foams*

Bubble size correlations presented in the literature were applied to ceramic foams. In particular, the Sauter mean bubble size, d_{32}, was plotted as a function of the mean energy dissipation and Weber number. It is worth noting that the correlations, as in the case of the gas hold-up correlations, refer to liquid–liquid systems or gas–liquid systems. In addition, as previously stated, the physical properties of the slurry change over the duration of the experiment due to foam formation so the density and viscosity of the initial slurry were used for the calculation of the Weber number. The Weber number is expected to increase during the course of the experiment due to the reduction in surface tension as the modified particles attach at the air–water interface; a quantification of the reduction in surface tension was not possible due to the nature of the system. Given these limitations, it was expected that the relationships would still describe the change in bubble size under the different operating conditions, although some discrepancies in terms of the exponent values were forecast.

Fig. 7 shows the normalised Sauter mean diameter, d_{32}/D, plotted as a function of both the mean energy dissipation and Weber number. Since the bubble size is affected by both the mean sparger pore size and the impeller diameter, different symbols were used for each enabling the effects to be examined separately.

Fig. 7 shows that the experimental data were fitted by the relationships proposed in the literature (Eqs. (6) and (7)) but, as expected, different values of the mean energy dissipation and Weber number exponents were necessary to correlate the data. The exponents derived in this work ranged from 0.10 to 0.33; these values are not significantly different from the value observed by Hu et al. (2006,2003) in systems where the presence of solvents strongly suppressed coalescence; the authors proposed a value of 0.35 for the exponent. The stability of the foams under consideration is due to the attachment of hydrophobic particles at the air-liquid interface which prevent coalescence. Table 4 summarises the values of the exponents reported in the literature and the values proposed in this work.

In Section 4.1, it was shown that the flow regime affects the porosity of the foam; a similar effect was observed for bubble size. Fig. 8(a) and (b) show the values of d_{32}/D for the different flow regime conditions for the 40 μm and 100 μm sparger disks respectively.

Table 4 – Comparison between the exponent values in correlations reported in the literature for bubble size (d_{32}) with values found in this study.

Correlation	Parameter & exponent	Literature value	Value from this study
Kolmogoroff (1949) Eq. (6)	ε^{β}	$\beta = -0.4$	$\beta = -0.22 \pm 0.12$
Hinze (1955) Eq. (7)	We^{γ}	$\gamma = -0.6$	$\gamma = -0.22 \pm 0.08$
Hu et al. (2006, 2003) Eq. (7)	We^{γ}	$\gamma = -0.35$	$\gamma = -0.22 \pm 0.08$

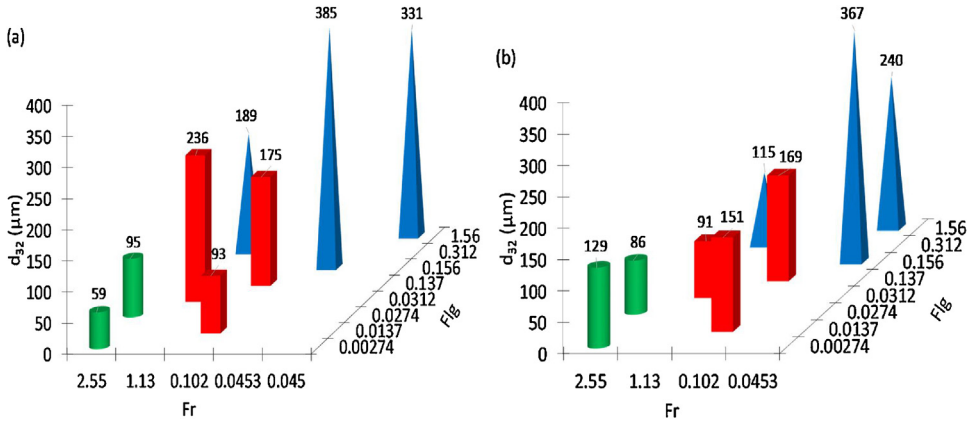

Fig. 8 – d_{32}/D depending on the different flow regimes conditions for (a) 40 μm sparging disk (b) 100 μm sparging disk. The different flow regimes are represented as flooded (▲), loaded (■) and fully recirculated (●).

From Fig. 8, it can be seen that a clear trend exists with smaller bubbles obtained under fully recirculating conditions and larger bubbles progressively formed when moving from loaded to flooded. It is notable that, contrary to expectation, the smaller porosity sparger disk produces bigger bubbles for foams made at Fl_g higher than ~0.02. At high gas flow rates, a higher level of coalescence is exhibited in the smaller porosity sparger; this is mostly due to the close proximity of the smaller pores and results in the formation of larger bubbles than those initially formed by the large porosity sparger.

4.4. *Rheological characterization of wet ceramic foams*

The effect of drop size and their distribution on the rheology of emulsions is well reported in the literature (Derkach, 2009; Masalova and Malkin, 2007). Due to the similarities between ceramic foams and emulsions, a correlation between the rheology of the foams produced under different mixing conditions and bubble size distribution was expected. The existence of such a correlation would allow an at-line measurement technique to be developed to control the foam structure during manufacture. The foams rheology was determined using the procedures described in Section 2.6 with all the measured samples presenting shear thinning behaviour. Fig. 9(a) compares the upwards (increasing shear rate) rheology curves for the 16 foams evaluated. There is a notable "kink" present in all the curves. Fig. 9(b) shows the upward (increasing shear rate) and downward (decreasing shear rate) rheology curve for the foam produced in run 4. The downward curve does not reach the initial viscosity of the fresh foam suggesting that the structure of the foam was irreversibly changed at the higher shear rates. In addition, the "kink" appears at lower shear rates in the down curve compared to the up curve. The different position of the "kink" might be used to develop a correlation if it could be shown that was not an artefact of the test procedure. One possibility was that slip was developing during the test despite the upper hatched plate geometry being used.

To investigate the nature of the inflection, the rheology of a foam was measured using three different geometries; a 40 mm steel plate, a 40 mm acrylic hatched plate and a rotor-vane geometry. In this case, a 20%$_{w/w}$ titania foam was produced using DL-phenylalanine as amphiphile. This change was implemented because the original amphiphile gave an unpleasant odour. In the phenylalanine system titania replaced the original alumina particles due to its better performance. Although the measured system was different from the original foams, the aim of the comparison was to evaluate the nature of the observed "kink". It was found that the extent of the inflection was geometry dependent, reducing when the vane was used compared with the parallel plate, suggesting that slip is occurring. Given the limitations of the experiment (odour and volume) the vane geometry could not be used for the DoE formulations. The stabilized bubbles in ceramic foams can be assumed to behave as soft spheres, thus, at high concentrations and low shear stress, they exhibit viscoelastic and solid-like behaviour but yield and flow above a yield stress (Fernandez-Neives et al., 2011). Slip of soft particles has been widely investigated in the literature; this occurs when particles are depleted from a solid surface giving a low viscosity boundary layer between the surface and the particles in the bulk of the suspension (Barnes et al., 1995).

The data presented in Fig. 9(a) can be extended allowing study of both the upward and downward shear rate ramp data; the samples can be divided into three groups where their behaviours are similar based on the kink location in terms of the slip onset shear rate and stress. This analysis is shown in Fig. 10 along with the corresponding bubble size data. Fig. 10 shows the sets of rheology curves having similar behaviour and the bubble size distribution of the corresponding foams; the figure indicates that foams having similar bubble size distribution present comparable shear rate values at which the "kink" appears. Table 3 reports the properties of the foam; the span values reported in the table refers to the width of the bubble size distribution calculated using (Merkus, 2009):

$$Span = \frac{D_{v0.9} - D_{v0.1}}{D_{v0.5}} \quad (17)$$

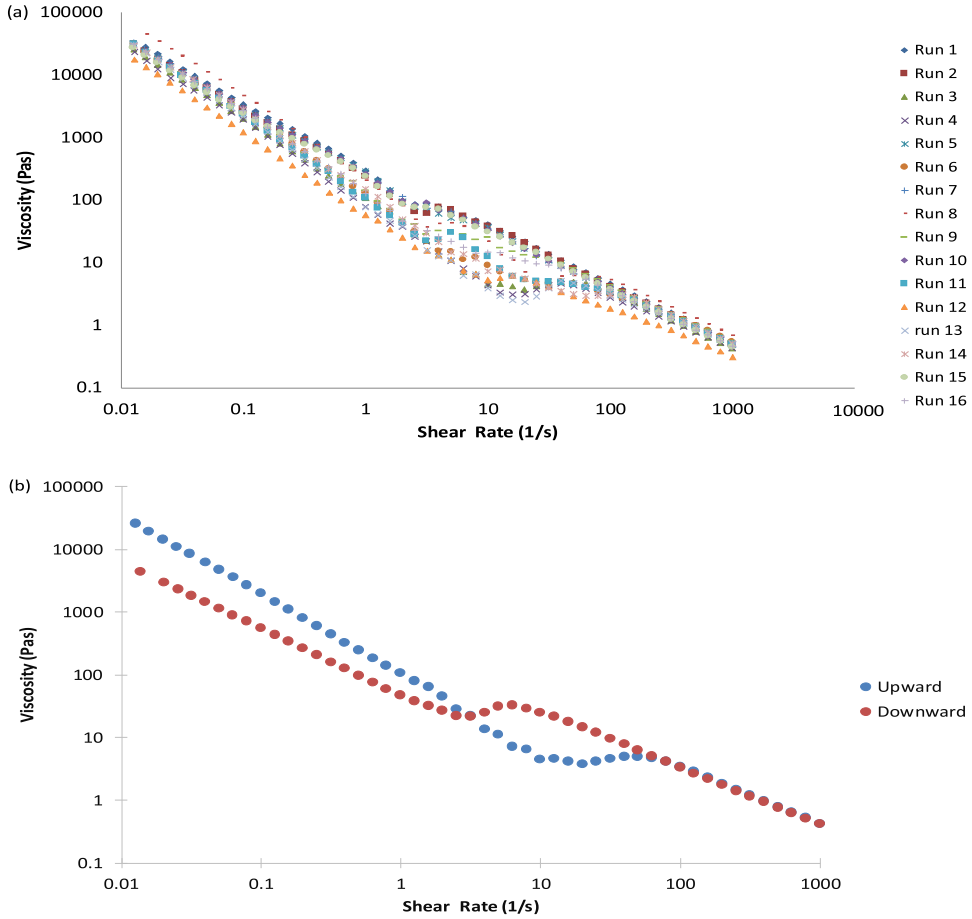

Fig. 9 – (a) Comparison of the upward rheology curve for the produced foams (b) details of the upward and downward rheology curve for foam made in run 4.

Table 5 – Summary of the foams properties divided by overlapping series.

	Exp.	d_{32}(μm)	Distribution span	Shear rate (s^{-1})	Shear stress (Pa)
1st set	1	367	4.08	2.51	214.9
	2	150	2.48	2.51	162.4
	5	236	5.08	2.51	195.0
	7	169	2.74	3.16	235.6
	10	331	2.95	2.51	210.7
	15	93	1.62	2.51	173.1
Average		224	3.16	2.62	198.6
2nd Set	3	95	1.56	9.99	44.9
	4	189	2.31	12.59	42.1
	12	129	1.50	10.01	53.6
	13	86	1.60	19.97	39.9
	14	114	1.70	12.59	73.6
Average		123	1.73	13.03	50.8
3rd Set	6	59	1.26	5.01	70.8
	8	240	2.43	3.98	118.9
	9	91	1.89	3.98	89.3
	11	175	1.83	3.16	71.1
	16	384	5.13	3.16	112.9
Average		190	2.51	3.86	92.6

It can be seen that slip occurs at different shear rate values in the three sets. In the first, slip appears at around 2.60 s^{-1}, in the second slip occurs at approximately 13.00 s^{-1} and in the third one slip occurs at around 3.90 s^{-1}. Although, the slip of the foams belonging to the same set occurs at very similar shear rates, due to the differences in viscosity among the compared foams, it is more indicative to compare the shear stresses at which slip occurs; these are summarized in Table 5.

Fig. 11 shows the dependence of the shear stress at which slip occurs on both Sauter mean diameter and distribution span.

Fig. 11 shows that a higher shear stress is necessary to generate slip when larger bubbles with wider distribution spans are present, thus onset of slip depends on the structural properties of the foam. Meeker et al. (2004a, 2004b) proposed that slip in soft particles systems is based on an elastohydrodynamic lubrication (EHL) mechanism which occurs when soft particles deform and develop flat facets at hard surfaces under

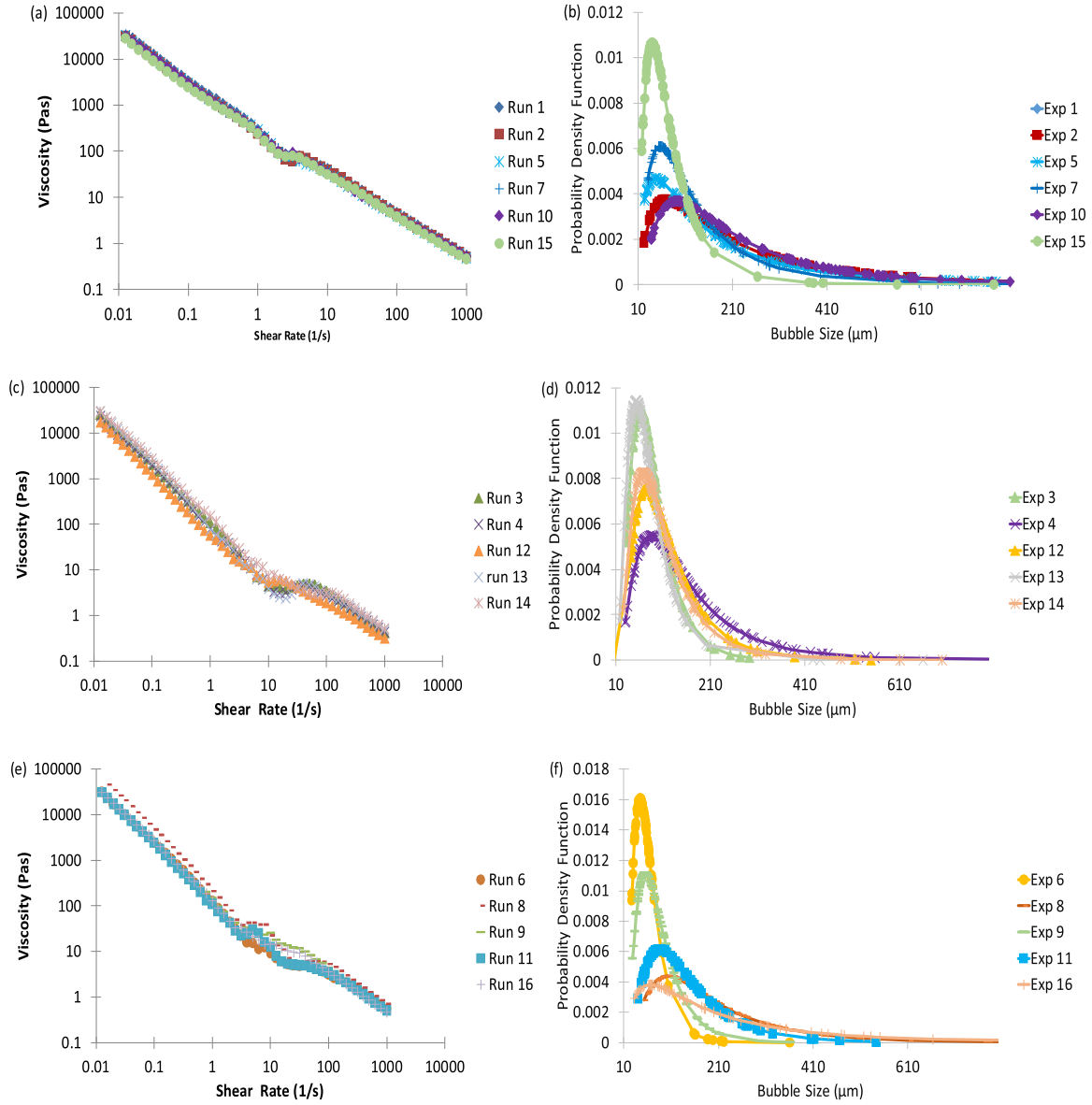

Fig. 10 – Series of rheology curves presenting similar behaviour and corresponding bubble size distribution: (a) first series of rheology curves (b) bubble size distribution of the foams in the first series (c) second series of rheology curves (d) bubble size distribution of the foams in the second series (e) third series of rheology curve (f) bubble size distribution of the foams in the third series.

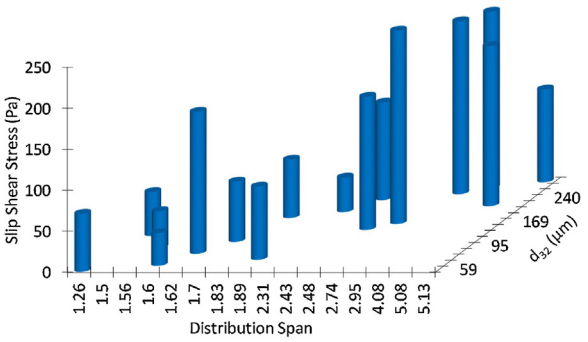

Fig. 11 – Slip shear stress as a function of bubble size and distribution span.

shear. The increased effective area of the particles promotes hydrodynamic lubrication with the thickness of the slip layer depending on the balance between lift force and the repulsive forces generated by the tendency of the particles to regain sphericity; these forces are dependent on the particles elastic modulus. The elastic modulus of bubbles can be described by the Gibbs elasticity term expressed as (Bianco and Marmur, 1993):

$$E = 2\frac{d\sigma}{dlnA_t} \tag{18}$$

where σ is the gas–liquid interfacial tension and A_t is the total surface area of the bubble which is, in turn, radius dependent. Although it was not possible to determine the value of the elasticity modulus due to the nature of the system, these relationships describe the dependence of slip on bubble size and appear to support the observed behaviour.

The viscoelastic properties of the foams were determined following the testing procedure reported in Section 2.6. All the foams presented a similar trend so, for brevity, only oscillation curve for foam produced in run 4 is presented in Fig. 12.

It should be noted that ceramic foams present quite an extensive linear viscoelastic region (LVER). In the LVER G′ presents higher values with respect to G″ indicating that the

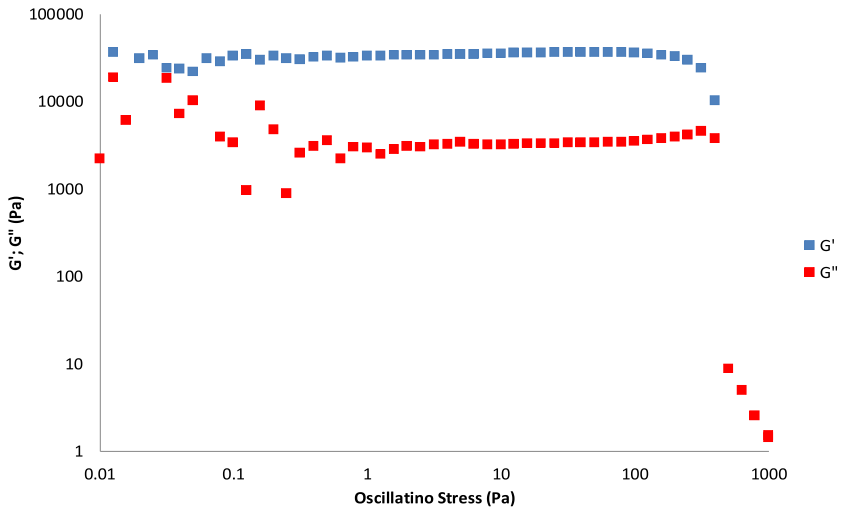

Fig. 12 – Amplitude sweep curve for the foam produced in run 4.

ceramic foams behave more like an elastic solid. All the foams presented a LVER which extended beyond 100 Pa with the foam from experiment 8 extending to 500 Pa. The end of the LVER can be used as an indication of the maximum stress at which the foam can be subjected without destroying its structure. In fact, it has already been mentioned that particles stabilised foams behave like soft spheres giving a solid-like behaviour to the foam. It is expected that as the stabilized bubbles are broken, the foams behaves more like a viscous fluid. This aspect could be particularly relevant in the foam post-processing (e.g. extrusion or forming), where the material could be subjected to stresses higher than those experienced during its manufacture. In these operations knowing the maximum stress at which the foam can be subjected without destroying its structure is fundamental to retain the required product specifications.

5. Conclusions

In this work, the manufacturability of ceramic foams has been studied; in particular, the process parameters affecting the foam properties have been identified and include porosity and bubble size distribution. The effects of impeller speed, impeller diameter, gas flow rate, sparging time and sparging disk mean pore size have been investigated through design of experiment (DoE) in which foam density, foam porosity, foam stability and bubble size distribution were selected as responses. From the experimental work, it was established that foam stability is not dependent on its manufacturing process but is only affected by the initial ceramic slurry formulation. It was determined that sparging time, air flow rate and impeller speed are the major factors affecting foam density and porosity while impeller speed, impeller diameter and the interactions between sparging time and air flow rate and between impeller diameter and the mean pore diameter of sintered disk have an impact on bubble size. To facilitate the process scale-up, foam porosity and foam bubble size distribution were plotted as functions of different global mixing parameters. Correlations capable of describing the investigated system were not found in the literature, this was due to the transient flow behaviour of the investigated system and the change in its physical properties during the foaming. The system was better described by equations valid for turbulent systems and those were used to correlate foam porosity and bubble size to dimensionless numbers describing the studied system. As expected, in both cases, differences in the exponent values were found compared to literature but the used relationships were well correlated by the experimental data. It is important to remark that, due to the complexity of the system and the number of assumptions made during the study, the new exponents are relevant exclusively for the current system and future work is necessary to identify a general correlation.

To characterize the structure of the foam, rheological measurements were carried out. Slip was observed in the rheological data whose onset was dependent on foam structure as measured by the mean Sauter diameter and distribution span. The viscoelastic properties of the foams were also investigated through an amplitude sweep test showing that foams behave more like viscoelastic solids with the end of the linear viscoelastic region occurring over 100 Pa.

This study highlighted the complexity of the manufacturing process of ceramic foams. Nonetheless, relationships proposed in the literature were shown to be able, upon adjustment of the exponents, to correlate the experimental data. This allows the manufacturing process to be tuned to the desired foam structure. The existence of a correlation between foam rheology and its structural properties, such as bubble size and distribution, could be the starting point to develop an at-line measurement to check the evolution of the foam structure during its manufacture.

Acknowledgements

AC was funded by an EngD studentship from the EPSRC Industrial Doctorate Centre in Formulation Engineering at the University of Birmingham (EP/G036713/1) and Johnson Matthey plc. The authors would like to acknowledge Dr Chandresh Malde and Dr Sam Wilkinson at Johnson Matthey for useful discussion and input on the rheology work.

References

Albright, L.F., 2009. Albright's Chemical Engineering Handbook. Taylor & Francis Group LLC.

Anon, 2012. JMP 10 Modeling and Multivariate Method. SAS Institute, Cary.

Bach, H.F., Pilhofer, T., 1978. Variations of gas hold-up in bubble columns with physical properties of liquids and operating parameters of column. Ger. Chem. Eng. 1, 270–275.
Barnes, H.A., Bonnecaze, R.T., Cloitre, M., 1995. A review of the slip (wall deplation) of polymer solutions, emulsions and particles suspensions in viscometers: its cause, character, and cure. J. Non-Newton. Fluid Mech. 56, 221–251.
Benhkish, A., Lemoine, R., Sehabiague, L., Oukaci, R., Morsi, B.I., 2007. Gas holdup and bubble size behaviour in a large-scale slurry bubble column reactor operating with an organic liquid under elevate pressures and temperatures. Chem. Eng. J. 128 (2–3), 69–84.
Bhaga, D., Pruden, B.B., Weber, M.E., 1971. Gas holdup in bubble column containing organic liquid mixtures. Can. J. Chem. Eng. 49, 417–420.
Bianco, H., Marmur, A., 1993. Gibbs elasticity of a soap bubble. J. Colloid Interface Sci. 158, 295–302.
Buffo, A., Alopaeus, V., 2016. Experimental determination of size distribution: analyzing proper sample size. Meas. Sci. Technol. 27, 1–6.
Calabrese, R.V., Francis, M.K., Mishra, V.P., Phongikaroon, S., 2000. Measurements and analysis of drop size in a batch rotor-stator mixer. In: 10th European Conference on Mixing, Delft, The Netherlands, pp. 149–156.
Colombo, P., Sheffled, M., 2005. Cellular Ceramics: Structure, Manufacturing, Properties and Applications. Wiley-VCH, Weihheim.
Derkach, S.R., 2009. Rheology of emulsions. Adv. Colloid Interface Sci. 151, 1–23.
Fernandez-Neives, A., Wyss, H., Mattson, J., Weitz, D.A., 2011. Microgel Suspensions: Fundamentals and Applications. Wiley-VCH Verlag.
Frohn, A., Roth, N., 2000. Dynamics of Droplets. Springer Science & Business Media.
Gauckler, L.J., Waeber, M.M., Contiand, C., Jacobduliere, M., 1985. Ceramic foam for molten-metal filtration. J. Metals 37 (9), 47–50.
Gonzenbach, U.T., Studart, A.R., Tervoort, E., Gauckler, L.J., 2006. Stabilization of foams with inorganic colloidal particles. Langmuir 22, 109383–109388.
Gonzenbach, U.T., Studart, A.R., Tervoort, E., Gauckler, L.J., 2007. Tailoring the microstructure of particle-stabilized wet foams. Langmuir 23, 1025–1032.
Greaves, M., Barigou, M., 1990. Estimation of gas hold-up and impeller power in a stirred vessel reactor. Fluid Mixing III 108, 235–255.
Harnby, N., Edwards, M.F., Nienow, A.W., 2001. Mixing in the Process Industries, 2nd Edition. Butterworth-Heinemann, Oxford.
Heijnen, J.J., Van't Riet, K., 1984. Mass transfer, mixing and heat transfer phenomena in low viscosity bubble column reactors. Chem. Eng. J. 28, B21–B42.
Hikita, H., Asai, S., Tanigawa, K., Segawa, K., Kitao, M., 1980. Gas hold-up in bubble columns. Chem. Eng. J. 20, 59–67.
Hinze, J.O., 1955. Fundamentals of the hydrodynamic mechanism of splitting in dispersion processes. AIChE J. 1, 289–295.
Hu, B., Nienow, A.W., Pacek, A.W., 2003. The effect of sodium caseinate concentration and processing conditions on bubble sizes and their break-up and coalescence in turbulent, batch air/aqueous dispersions at atmospheric and elevated pressures. Colloids Surf. B Biointerfaces 31, 3–11.
Hu, B., Pacek, A.W., Stitt, E.H., Nienow, A.W., 2005. Bubble sizes in agitated air-alcohol systems with and without particles: turbulent and transitional flow. Chem. Eng. Sci. 60, 6371–6377.
Hu, B., Nienow, A.W., Stitt, E.H., Pacek, A.W., 2006. Bubble size in agitated solvent/reactant mixtures used in heterogeneous catalytic hydrogenation of 2-butyne-1,4-diol. Chem. Eng. Sci. 61, 6765–6774.
Hughmark, G.A., 1967. Holdup and mass transfer in bubble columns. Ind. Eng. Chem. Process. Des. Dev. 6, 218–220.
Kasprzyk-Hordern, B., 2004. Chemistry of alumina, reactions in aqueous solution and its application in water treatment. Adv. Colloid Interface Sci. 110, 19–48.
Kastanek, F., Zahradnik, J., Kratochvil, J., Cermak, J., 1984. Modelling of large-scale bubble column reactors for non-ideal gas–liquid systems. In: Frontier in Chemical Reaction Engineering. John Wiley and Sons, New Delhi, India, pp. 330–344.
Khopkar, A.R., Kasat, G.R., Pandit, A.B., Ranade, V.V., 2006. Computational fluid dynamics simulation of the solid suspensionin a stirred slurry reactor. Ind. Eng. Chem. Res. 45, 4416–4428.
Kolmogoroff, A.N., 1949. Dokl. Akad. Nauk S.S.S.R. (N.S.) 66, 825.
Lau, R., Peng, W., Valazquez-Vargas, G., Yang, G.Q., Fan, L.S., 2004. Gas-liquid mass transfer in high-pressure bubbles columns. Ind. Eng. Chem. Res. 43, 1302–1311.
Lenth, R.V., 1989. Quick and easy analysis of unreplicated factorials. Technometrics 31, 469–473.
Machon, V., Pace, A.W., Nienow, A.W., 1997a. Bubble sizes in electrolyte and alcohol solutions in a turbolent stirred vessel. TransIChemE 75 (A), 339–348.
Machon, V., Pacek, A.W., Nienow, A.W., 1997b. Bubble sizes in electrolyte and alcohol solutions in a turbolent stirred vessel. TransIChemE 75 (A), 339–348.
Masalova, I., Malkin, A.Y.A., 2007. Peculiarities of rheological properties and flow of higly concentrated emulsions: the role of concentration and droplet size. Colloid J. 69 (2), 185–197.
Meeker, S.P., Bonnecaze, R.T., Cloitre, M., 2004a. Slip and flow in pastes of soft particles: direct observation and rheology. J. Rheol. 48, 1295–1320.
Meeker, S.P., Bonnecaze, R.T., Cloitre, M., 2004b. Slip and flow in soft particles pastes. Phys. Rev. Lett. 92 (19), 4.
Merkus, H.G., 2009. Particles Size Measurements: Fundamentals, Practise, Quality. Springer.
Montante, G., Magelli, F., 2005. Modelling of solids distribution in stirred tanks: analysis of simulation strategies and comparison with experimental data. Int. J. Comput. Fluid Dyn. 19 (3), 253–262.
Nienow, A.W., Wisdom, D.J., Middleton, J.C., 1978. Proceedings of 2nd European Conference on Mixing. BHRA Fluid Engineering, Cranfield, pp. pp. F1-1-F1-16 and X54.
Nienow, A.W., Hu, B., Pacek, A.W., 2003. Bubble sizes in stirred reactors: what can we predict? Annual Meeting, Paper 361a.
Ozturk, S.S., Schumpe, A., Deckwer, W.D., 1987. Organic liquids in bubble column: holdups and mass transfer coefficients. AIChE J. 33, 1473–1480.
Paul, E.L., Atiemo-Obeng, V.A., Kresta, S.M., 2004. Handbook of Industrial Mixing: Science and Practice. Wiley-Interscience, Hoboken, NJ.
Pinelli, D., Nocentini, M., Magelli, F., 2001. Solids distribution in stirred slurry reactors: influence of some mixer configurations and limits to the applicability of a simple model for predictions. Chem. Eng. Commun. 00, 1–18.
Rewatkar, V.B., Deshpande, A.B., Pandit, A.B., Joshi, J.B., 1993. Gas hold-up behaviour of mechanically agitated gas–liquid reactors using pitched blade downflow turbines. Can. J. Chem. Eng. 71, 226–237.
Sada, E., Kamazawa, H., Lee, C.H., 1983. Chemical absorption in bubble column loading concentrated slurry. Chem. Eng. Sci. 38, 2047–2051.
Sarrafi, A., Jamialahmadi, M., Muller-Steinhagen, H., Smith, J.M., 1999. Gas holdup in homogeneous and heterogeneous gas–liquid bubble column reactors. Can. J. Chem. Eng. 77, 11–21.
Shinnar, R., 1961. On the behaviour of liquid dispersions in mixing vessels. J. Fluid Mech. 10, 259.
Smith, J.M., 1991. Simple performance correlations for agitated vessels. Proc. 7th Euro Congress on Mixing, 233–241.
Sprow, F.B., 1967. Drop size distributions in strongly coalescing agitated liquid–liquid systems. AIChE J. 13 (5), 995–998.
Studart, A.R., Gonzenbach, U.T., Tervoort, E., Gauckler, L.J., 2006. Processing routes to macroporous ceramics: a review. J. Am. Ceram. Soc. 89 (6), 1771–1789.
Whitton, M.J., Nienow, A.W., 1993. Scale-up correlations for gas hold-up and mass transfer coefficients in stirred tank

reactors. Proc. 3rd Int. Conference on Bioreactor and Bioprocess Fluid Dynamics, 135–149.
Wilkinson, P.M., Spek, A.P., van Dierendonck, L.L., 1992. Design parameters estimation for scale-up of high-pressure bubble columns. AIChE J. 38, 544–554.
Williams, A., Garner, C.P., Binner, J.G.P., 2008. Measuring Pore Diameter Distribution of Gelcast Ceramic Foams from Two-Dimensional Cross Sections. Loughborough's Institutional Repository.
Wong, J.C.H., Tervoort, E., Busato, S., Gauckler, L.J., Ermanni, P., 2011. Controlling phase distributions in macroporous composite materials through particle-stabilized foams. Langmuir 27, 3254–3260.
Yawalkar, A.A., Pangarkar, V.G., Beenackers, A.A.C.M., 2002. Gas hold-up in stirred tank reactors. Can. J. Chem. Eng. 80, 158–166.
Ye, K.Q., Hamada, M., 2000. Critical values of the length method for unreplicated factorial designs. J. Qual. Technol. 32 (1), 57–66.
Zou, R., Jiang, X., Li, B., Zu, Y., Zhang, L., 1988. Studies on gas holpup in a bubble column operated at elevated temperatures. Ind. Eng. Chem. Res. 27, 1910–1916.